Pergamon

Geochimica et Cosmochimica Acta, Vol. 66, No. 2, pp. 213–221, 2002

0016-7037/02 $22.00 + .00

PII S0016-7037(01)00771-2

Modification of olivine surface morphology and reactivity by microbial activity during chemical weathering

SUSAN A. WELCH[1] and JILLIAN F. BANFIELD,[1,*]

[1]Dept. Geology and Geophysics, UW Madison, 1215 West Dayton St., Madison, WI 53706 U.S.A.

(*Received June* 9, 2000; *accepted in revised form June* 8, 2001)

Abstract—Prior transmission electron microscope studies showed that the surface geometry of olivine changes dramatically during natural chemical weathering. However, similar morphological evolution has not been reported in laboratory studies of olivine dissolution. In this study, we examined the development of fayalite (Fe_2SiO_4) surface morphology during both abiotic and biotic (using *Acidithiobacillus ferrooxidans*) laboratory dissolution experiments at an initial pH of 2.0. The fayalite came from Cheyenne Canyon, Colorado (Smithsonian # R 3516) and contains a few percent laihunite (olivine structure with ordered ferric iron and vacancies, $\sim Fe^{2+}_{0.8}Fe^{3+}_{0.8}SiO_4$). High-resolution field emission low voltage scanning electron microscope (SEM) characterization of all reacted samples showed etch patterns consistent with those reported from naturally reacted olivine. High-resolution transmission electron microscope (HRTEM) data demonstrated pervasive channeling on (001), with channel spacings that range down to < 10 nm. Formation of channels on (001) is probably initiated by preferential removal of cations from olivine M1 sites. Channeling confers at least an order of magnitude increase in surface area. Relict strips of olivine between channels contain laihunite layers that are oriented parallel to channel margins. X-ray diffraction analyses indicated that the relative abundance of laihunite is higher in reacted compared to unreacted samples. This result is consistent with prior studies of naturally weathered olivine that suggest that laihunite is far less readily dissolved than olivine.

Samples reacted in the presence of *A. ferrooxidans* cells that enzymatically oxidized iron, or in solutions where ferric iron was added to simulate biological activity, dissolve at a much slower rate than samples reacted abiotically. We attribute suppression of the olivine dissolution rate to surface adsorption of Fe^{3+}. It is probable that ferric iron adsorption is controlled by M2 sites in the underlying olivine structure. If this is coupled with removal of M1 cations during channel formation, then a modified laihunite-like surface will develop (vacancies in laihunite are on M1 sites). Although surface modification might only penetrate a few atomic layers, an inherently unreactive laihunite-like surface structure could explain both the pervasive channeling and the dramatic suppression of the measured dissolution rate. *Copyright © 2002 Elsevier Science Ltd*

1. INTRODUCTION

Microorganisms and microbial processes can impact the weathering rates of Fe-silicate rich rocks (Thorseth et al., 1992; 1995; Fisk et al., 1998; Liermann et al., 2000). Simultaneously, ferrous iron released by dissolution of Fe-silicates may represent a significant energy source for chemolithotrophic microorganisms, especially in extremely oligotrophic environments (Jakosky and Shock, 1998; Stevens and McKinley, 1995; McCollom and Shock, 1997). The rate of supply of ferrous iron to solution during Fe-silicate dissolution is pH dependent. Mineral reactions are most likely to sustain significant chemoautotrophic microbial populations if solutions are acidic.

Fluids associated with sulfide-rich deposits can be extremely acidic, and these frequently contain significant populations of Fe-oxidizing microorganisms. A subset of the microorganisms in these solutions is sustained by aqueous ferrous iron derived from sulfide mineral dissolution. However, reactions with surrounding silicate rocks could also liberate ferrous iron that can be utilized in microbial iron respiration. More importantly perhaps, enzymatic iron oxidation liberates ferric ions, and these could significantly modify the rates of the acid-neutralization reactions.

Although Fe-rich silicate mineral are very common in the Earth's surface rocks, few experimental studies have focused on the dissolution or weathering of these minerals due to complications from oxidative dissolution reactions and the subsequent precipitation of iron oxyhydroxide phases. Mineral dissolution experiments with Fe-rich silicate minerals demonstrate that oxidative dissolution can enhance or inhibit the dissolution reaction. Experiments by Hoch et al. (1996) showed that a ferrous iron-rich augite dissolved faster than an iron-poor diopside under similar experimental conditions. Increase in the dissolved oxygen concentrations from 0.6 to 1.5 ppm O_2 increased Si flux from augite by a factor of three, whereas oxygen concentration had no effect on diopside dissolution rates. Similarly, White and Yee (1985) studied the dissolution of several Fe-silicate minerals and attributed the increase in rate under oxidizing conditions to either dissolved oxygen or to Fe^{3+}. They suggested that these compounds were able to oxidize iron on the mineral surface, which resulted in a charge imbalance that increased the flux of other octahedrally coordinated cations to solution. In contrast, both Wogelius and Walther (1992) and Siever and Woodford (1979) noted a decrease in the long-term dissolution rate of fayalite that they attributed to the precipitation of iron oxyhydroxide phases. In all of these experimental studies, the extent of reaction was determined by the net release of material to solution; the evolution of mineral surface morphology was not considered.

* Author to whom correspondence should be addressed (jill@geology.wisc.edu).

Naturally weathered olivine is almost always pervasively channeled parallel to (001). Secondary mineral phases such as smectite, hematite, or goethite are commonly developed within the few nanometer-wide channels (e.g., Casey et al., 1993; Banfield et al., 1990; Banfield et al., 1991; Eggleton, 1984). The secondary minerals commonly have a topotactic relationship to the reacting olivine and largely fill the space previously occupied by olivine (Banfield et al., 1990). Consequently, the channels represent zones of limited fluid exchange with bulk weathering solutions.

Commonly, (001) channels in olivine are bounded by planar defects of laihunite, a silicate with an olivine-type structure. Vacancies in laihunite are typically ordered onto M1 sites and ferric iron onto M2 (see Janney and Banfield, 1998, and references therein). The pattern of vacancy ordering varies, giving rise to at least three polytypes (e.g., Kondoh et al., 1985; Shen et al., 1986). The general composition of laihunite can be represented as $V_xFe^{2+}_{2-3x}Fe^{3+}_{2x}SiO_4$, where V represents vacancies and x ranges from 0.24 to 0.5 (Kondoh et al. 1985). When laihunite develops in Mg-rich olivine, it adopts a composition $\sim (Fe^{2+},Mg^{2+})_{0.8}(Fe^{3+})_{0.8}SiO_4$ (Banfield et al., 1990). Laihunite has been produced experimentally by fayalite oxidation at elevated temperatures (300 to 800°C; e.g., Kondoh et al., 1985), but the full range of conditions under which it can form is unknown. Laihunite was initially reported in altered fayalite, but is now known to occur in a wide range of olivine compositions ($\sim Fo_{90}$–Fo_{50}; see Banfield et al., 1990; Banfield et al., 1992). During low temperature aqueous alteration, laihunite is significantly less reactive than fayalite (Banfield et al., 1990).

The purpose of this paper is to investigate the coupling between mineral dissolution and surface morphologic evolution during chemical weathering, and to evaluate the ways in which microbial activity impacts mineral surface reactivity. The dissolution textures produced by fayalite alteration in laboratory experiments are compared to naturally weathered fayalite from a fayalite bearing granite (Adirondack Mountains, New York) and to previously published data from naturally weathered olivines. An explanation for the impact of ferric iron on the fayalite dissolution rate is proposed.

2. MATERIAL AND METHODS

Natural fayalite was obtained from the Smithsonian Institution (R 3516). Sample R 3516 is from Cheyenne County, Colorado. Millimeter-sized crystal aggregates were crushed and sieved, and the 25 to 75μm-size fraction was used in experiments.

Experiments were conducted in the pH range 2 to 4 and utilized *Acidthiobacillus ferrooxidans* (previously known as *Thiobacillus ferrooxidans*), an acidophilic, iron-oxidizing, chemoautotrophic bacterium commonly cultured from pH 2 to 4 solutions. We chose these experimental conditions because although ferrous iron can also be utilized by microbial populations in microaerophilic, neutral pH niches, such organisms are notoriously difficult to study in the laboratory.

100 mg of 25 to 75 μm-sized fayalite was added to 50 to 100 mL of solution in polycarbonate flasks. Solutions consisted of a dilute medium (1 mM $NH_4(SO_4)_2$, 1 mM $NaHCO_3$, 100 μM KH_2PO_4) with initial pH adjusted to 2 with H_2SO_4 ($\sim$10 mM). Fayalite dissolved stoichiometrically at pH 2 in this medium at a rate that is closely comparable to fayalite dissolution rates reported previously (initial rate of $\sim 1.3 \times 10^{-11}$ moles Fe^{2+}/cm^2s; see Santelli et al., 2001). The biotic experiments had approximately 10^7 cells/mL of *A. ferrooxidans* added to the culture medium. Cells were separated from their growth medium by a series of filtrations, and cells were vigorously rinsed to remove adsorbed iron. The experiments to test the effects of chemical affinity

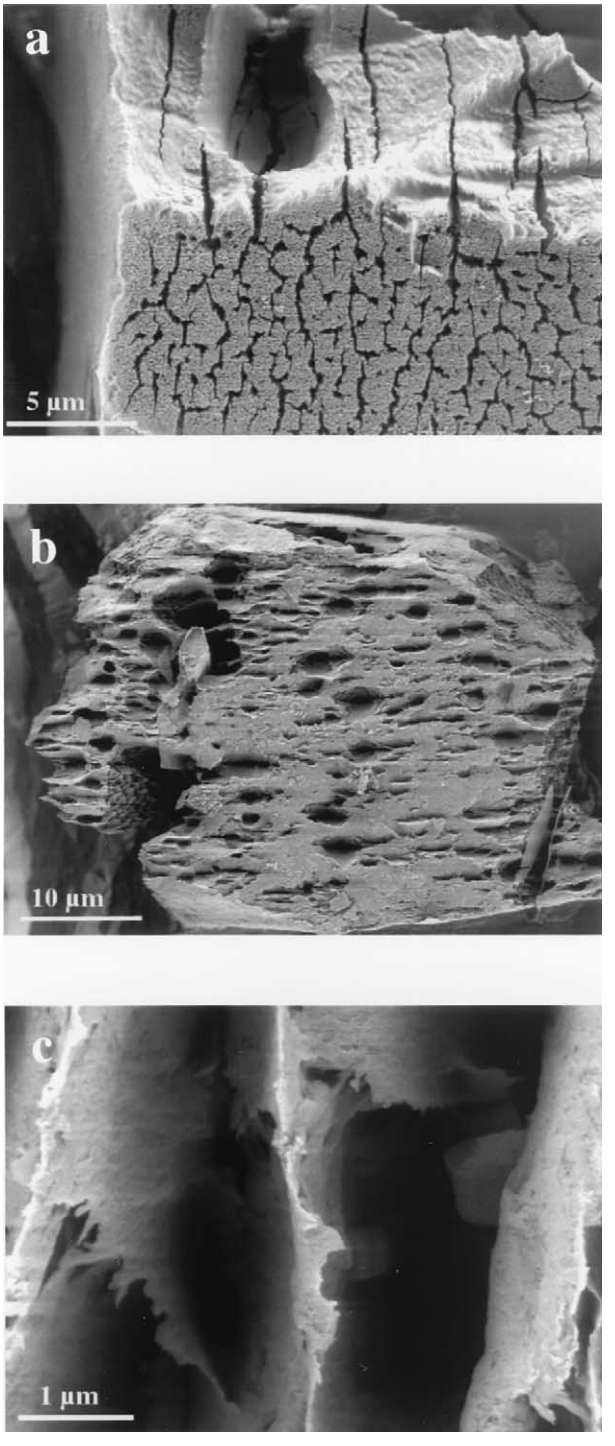

Fig. 1. Field emission high-resolution scanning electron microscope images of fayalite crystals after reaction in abiotic experiments at pH 2 for up to 2 weeks: (a) the top and front surfaces of this prismatic grain are intersected by deep etch pits that are oriented parallel to the third, relatively unreacted surface (left side of image). Comparison with TEM data (Fig. 4) confirms that the channels and the near-vertical, unreacted surface are parallel to (001). The front (vertical) surface displays additional deep pitting. (b) Highly reacted crystal exhibiting elongate lenticular pits. (c) Higher magnification image of a region of a highly reacted crystal showing thin strips of remaining material (XRD patterns confirm that this material is a mixture of fayalite and laihunite, see text).

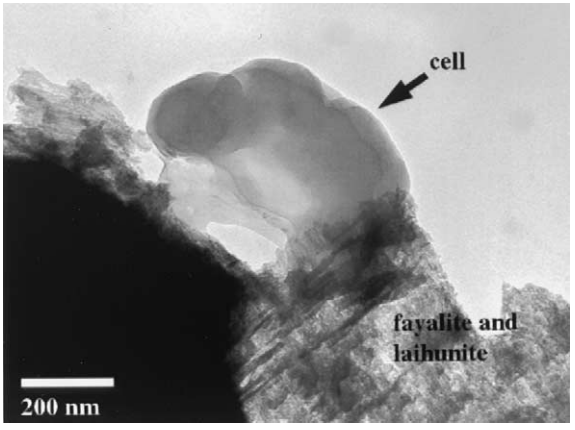

Fig. 2. Transmission electron microscope image of a fragment of fayalite reacted in the presence of *A. ferrooxidans* cells at pH 2. Close proximity between the cell and the altered silicate mineral is evident. This is expected because *A. ferrooxidans* derives metabolic energy via catalysis of oxidation of iron released by fayalite dissolution.

on fayalite dissolution contained 1mM Mg^{2+} or Fe^{2+} or Fe^{3+}, with an initial solution pH of 2. Flasks were placed on a rotary shaker at room temperature and solutions were sampled periodically. Experiments lasted approximately one to three weeks, depending on initial solution pH. Details are reported in Santelli et al. (2001).

At the end of the dissolution experiments, the mineral samples were gently rinsed with distilled water and a fraction of the mineral grains were placed on carbon tape on SEM stubs. Mineral samples were coated with either gold or platinum before examination in a Leo 982 low voltage high-resolution scanning electron microscope operated at 3 kV and ~ 4 mm working distance using an in lens secondary electron detector. Fayalite that had been reacted at pH 2 in the biologic experiments also was analyzed by TEM. Mineral grains were lightly crushed in a mortar and pestle, the mineral slurry was then suspended in distilled water and a drop was placed on a 200 mesh, formvar-coated copper grid. Samples were carbon coated and examined using a Philips CM200 Ultratwin Transmission Electron Microscope (0.2 nm point resolution) operated at 200 kV.

Samples of the Wanakena fayalite granite, central Adirondack Highlands, NY, were asceptically collected for mineralogical and microbiological analysis. Rock samples were split using sterilized knives and forceps and subsamples were placed on carbon tape on SEM stubs. Minerals were coated with either gold or platinum and then examined using the Leo 982 SEM.

For powder X-ray diffraction (XRD) analysis, unreacted and reacted samples were mounted on a low background quartz plate. XRD patterns were collected using a Scintag PADV automated powder diffractometer operated at 35 kV and 40 mA.

3. RESULTS

3.1. Abiotic Experiments

SEM examination of natural fayalite reacted without cells at an initial pH of 2 revealed that the material was extensively etched (Fig. 1). Approximately half of the starting material was dissolved over the course of the experiments. Figure 1a shows an SEM image of a reacted fayalite grain bounded by three surfaces that are approximately normal to each other. Two of the surfaces are very etched. One of these surfaces is intersected by deep, parallel channels and larger, open oval-shaped etch pits. The second is intersected by the same channels and is characterized by finer-scale, deep etching. The third surface, on the left side of the image, is relatively unreacted. Parallel etch channels and elongate pits with their long axes parallel to the

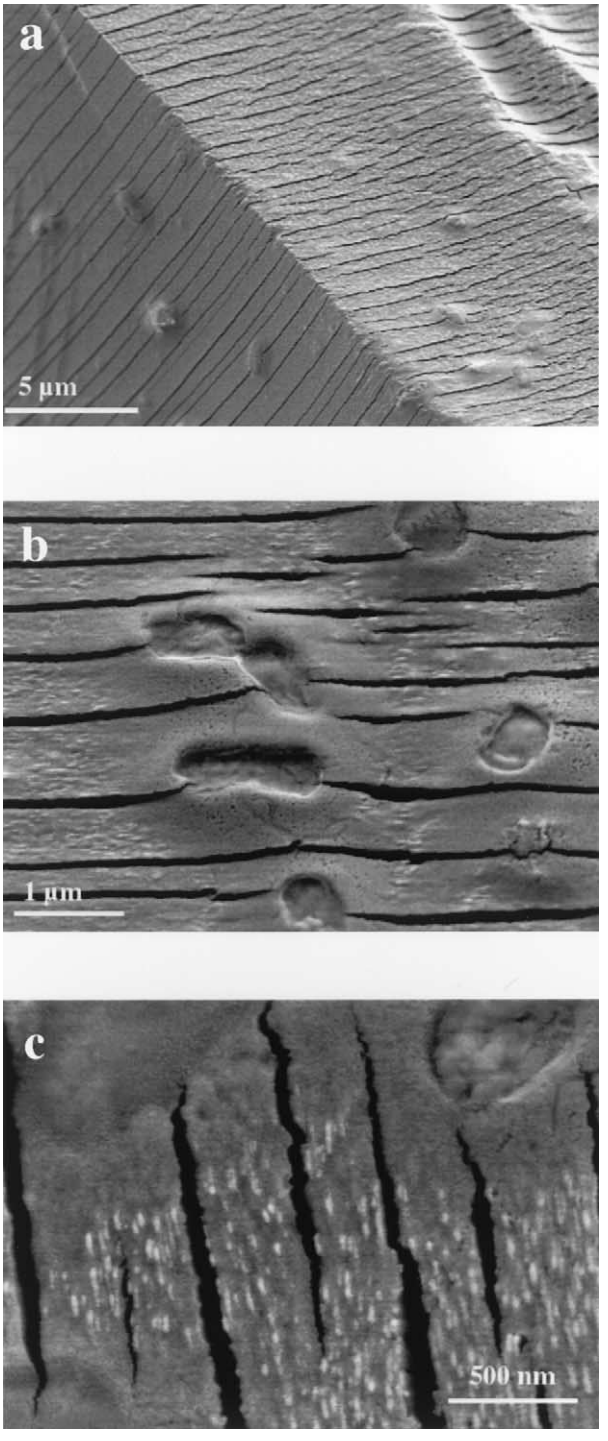

Fig. 3. Field emission high-resolution scanning electron microscope images of fayalite crystals reacted under the same conditions as those shown in Figure 1, but in the presence of active *A. ferrooxidans* cells. (a) Semiperiodically spaced channels intersecting two fayalite surfaces. Cells are visible as micron-sized bumps. Note that the crystals appear much less reacted than those shown in Figure 1a. Tens of grains examined all showed this "sliced loaf" appearance. (b) Higher magnification image showing cells (including one dividing pair) and surrounding polymer-bound mineral products on the reacted fayalite surface. (c) High magnification image of the etched surface in proximity to cells. Note the surface roughening, suggestive of finer-scale etching of the surface.

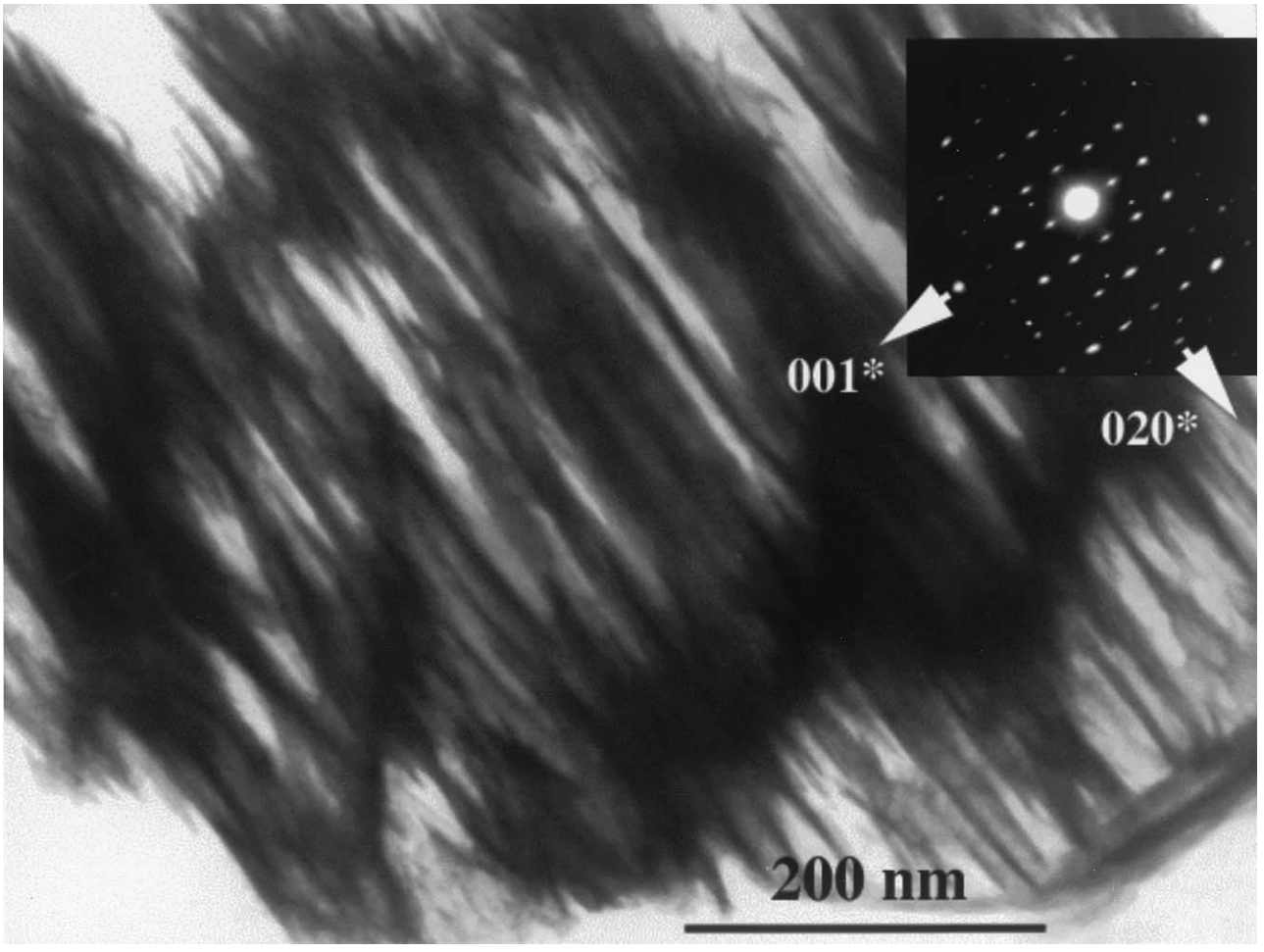

Fig. 4. TEM image of a fayalite grain reacted in the presence of microorganisms at pH 2. The fine scale subdivision by channels parallel to (001) is evident.

channels are common features (Fig. 1b). In highly reacted samples, these etch channels are only separated by thin (10s of nm wide) sheets of material (Fig. 1c).

3.2. Biologic Experiments

In biologic experiments *A. ferrooxidans* cells are often associated with the altered fayalite crystals (Figs. 2 and 3). Santelli et al. (2001) showed that the total amount of material released to solution by fayalite dissolution was about a factor of 5 less than in the abiotic experiments. The much slower rate of dissolution of fayalite in the presence of microorganisms is also evident when we compare SEM images of the biologically reacted fayalite (Fig. 3a–c) with images of fayalite reacted abiotically under otherwise identical conditions (Figs. 1a–c) for the same period of time.

SEM images suggest that fayalite dissolution in the biologic experiments is characterized by surface roughening and the formation of a narrow (few 10's nm wide), periodically spaced (approximately 500 nm to 2 μm apart) etch pits (Fig. 3). However, higher-resolution TEM characterization of reacted mineral grains revealed that the channels typically penetrate the entire crystal (Fig. 4). Figure 5 shows the reacted fayalite at high magnification. An $\sim$ 50 nm wide etch channel, such as are evident in SEM images of fayalite reacted in the biologic experiments (Fig. 5a), is apparent. Periodically spaced, 1 to 2 nm wide channels $\sim$ 10 nm apart are present parallel to the larger etch channels (Fig. 5a,b). The terminations of these 'fingers' are seen as surface roughness in some of the SEM images (Fig. 3c). TEM data (Fig. 4 and 5b) show that the channels are parallel to (001) olivine (thus the channels and relatively unreacted surface in Fig. 1a are parallel to (001)).

Details of high-resolution TEM images (Fig. 5) show that lattice fringe periodicities typical of olivine persist to within a fraction of a nanometer of the olivine surface. Although the surfaces of channels in fayalite appear to retain olivine structure, disordered vacancies and modified cation occupancy patterns may occur. The persistence of olivine-type structure indicates that the difference between the stoichiometry of solutions in biologic dissolution experiments and fayalite (Santelli et al., 2001) can not be attributed to formation of a substantial leached layer.

Ferric iron oxyhydroxides present in biologically reacted

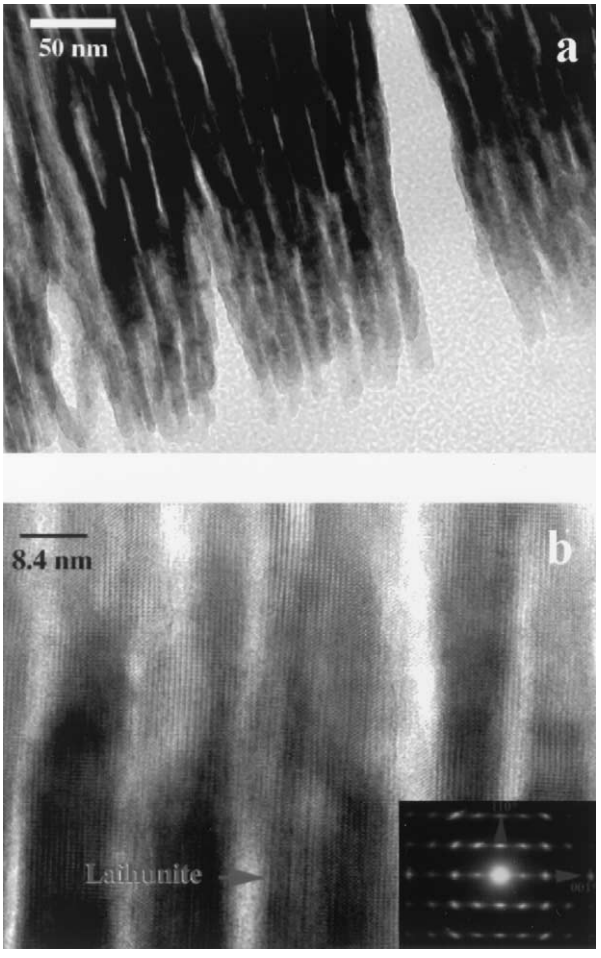

Fig. 5. High-resolution TEM images (a) showing that larger channels (as detected in SEM images such as in Fig. 3) are separated by many nanometer-scale channels. (b) Lattice fringe image showing modified contrast associated with every third (001) plane. In view of the streaking and splitting of reflections evident in the inset SAED pattern and prior TEM studies, this is attributed to ordering of ferric iron and vacancies, as found in laihunite.

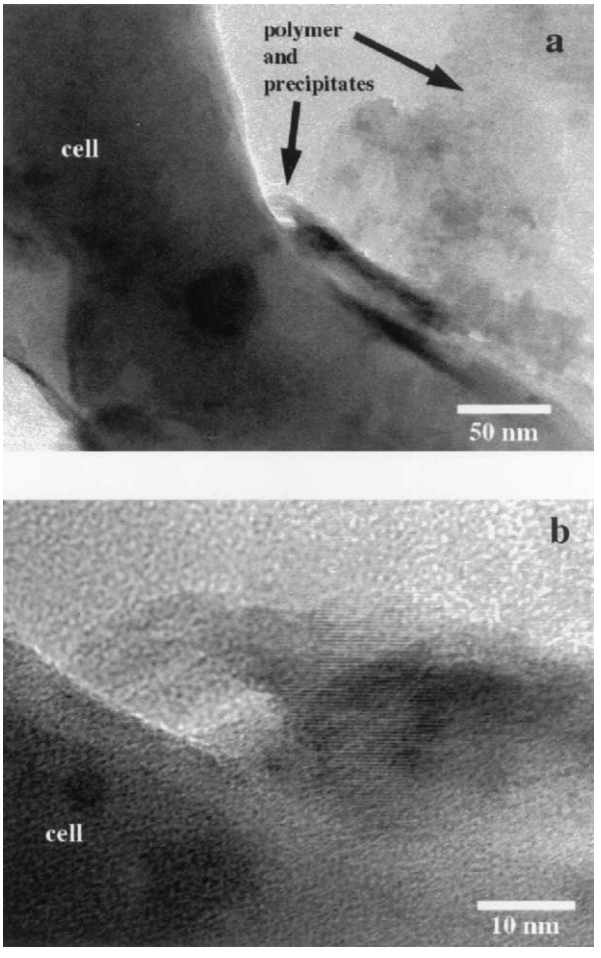

Fig. 6. TEM images of a portion of a *A. ferrooxidans* cell and its associated polymers (light contrast). Dark contrast in (a), indicated by a vertical arrow, is associated with an iron-rich precipitate. (b) High-resolution image of the precipitate in (a) showing lattice fringe periodicities that verify the crystallinity and indicate that the phase is goethite.

fayalite experiments were identified as ferrihydrite and goethite by measurement of ring diameters in selected area electron diffraction (SAED) patterns and using periodicities in high-resolution lattice fringe TEM images. Ferric oxyhydroxides occur as rounded or elongate, several nanometer long crystals that are concentrated in aggregates. These particles do not completely coat mineral surfaces. Some secondary minerals adhere to the surfaces of *A. ferrooxidans* cells (Fig. 6a,b). Lattice fringes indicate that these are crystalline; fringe spacings are consistent with their identification as goethite (Fig. 6b). These products are also evident in SEM images of the halo of polymers surrounding cells (Figs. 3b,c).

The SAED patterns (inserts in Figs. 4, 5b) from the mineral grains in Figure 3 show splitting of 00*l* reflections and streaking parallel to **c***. This is characteristic of laihunite layers within olivine (Banfield et al., 1990). Laihunite layers, visible in high-resolution TEM images due to the contrast changes resulting from ferric iron and vacancy ordering, are developed parallel to (001) olivine (Fig. 5b).

Powder X-ray diffraction patterns collected from the reacted material showed slight splitting of the 00*l* peaks, with small shoulder peaks at higher values of 2θ, consistent with the presence of laihunite (laihunite **c** = 5.801 Å compared to fayalite **c** = 6.09 Å). The relative intensity of 00*l* peaks from laihunite compared to 00*l* peaks from fayalite was clearly larger in reacted materials, but the low total intensity of the laihunite peaks precludes quantification.

3.3. Naturally Weathered Fayalite from Fayalite Granite

Several samples of the Wanakena fayalite granite were examined by SEM, visible light, and UV epifluorescence microscopy. Microorganisms (both prokaryotes and eukaryotes) were abundant on exposed mineral surfaces, although they did not appear to be preferentially associated with any specific mineral. Cell densities, estimated using epifluorescent microscopy, typically ranged from approximately a few to many tens of cells/10^4 μm^2 (approximately the field of view on the microscope at the highest magnification) on weathered samples. It was diffi-

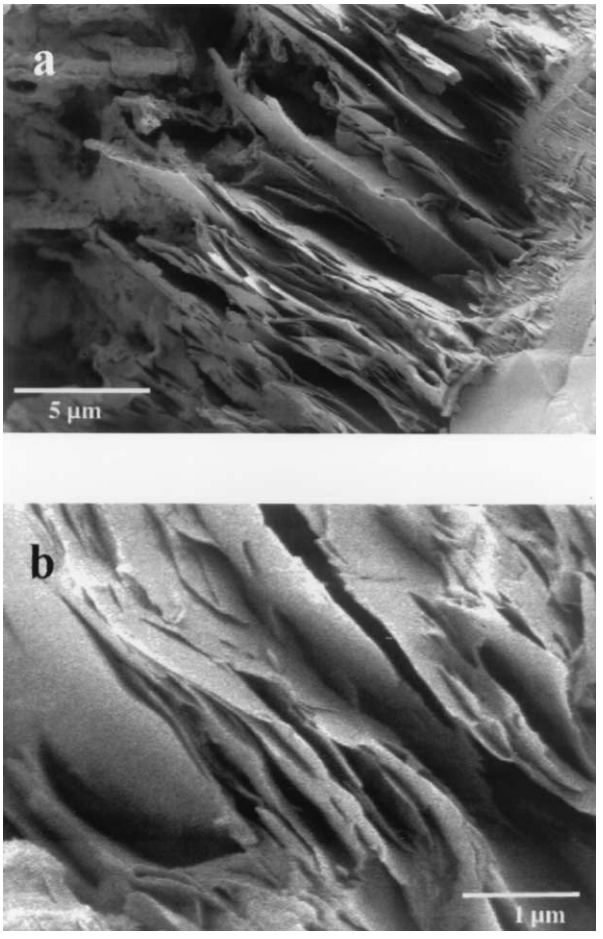

Fig. 7. SEM images of altered iron silicates in naturally weathered fayalite granite. The textures shown in (a), and at higher magnification in (b), are comparable to those observed in experimentally weathered fayalite.

cult to enumerate cells accurately due to the mineral surface roughness.

SEM data showed that fayalite grains exposed at the rock surface were highly weathered compared to other minerals exposed at the surface. Extensively weathered fayalite is finely divided, and exhibits dissolution textures similar to those generated in the abiotic dissolution experiments (Fig. 7).

4. DISCUSSION

Combination of TEM and SEM data for experimentally dissolved fayalite in abiotic and biologic experiments consistently indicates the predominant channel orientation is parallel to (001) (axes assigned in the P*bnm* space group). Thus, fayalite reacted under acidic conditions in both biologic and abiotic experiments exhibits textures that are very similar to those found in naturally weathered olivines with a wide range of Mg:Fe (Casey et al., 1993; Banfield et al., 1992; Banfield et al., 1990; Banfield et al., 1991) and in fayalite from the Adirondack samples (this study). To our knowledge, this is the first time microstructures essentially identical to those characteristic of naturally weathered minerals have been reported in an experimental olivine dissolution study.

Heterogeneous etch patterns on different surfaces of forsteritic olivine have been described by Awad et al. (2000). Their SEM images show some features similar to those reported here, although only one of their indexed grain orientations indicates channeling consistent with that reported in this study and by previous workers (two of their three oriented grains imply channels parallel to (100)). It is possible that the difference between dissolution features reported by Awad et al. (2000) and those described from naturally weathered samples arise due to differences in the mineral or solution characteristics. However, the similarities between fayalite reacted at pH 2 in this study and those naturally weathered in near neutral pH solutions suggests that the pit formation mechanism is not highly pH dependent.

It is important to note that experimental fayalite dissolution (and natural olivine weathering) involves subdivision of the olivine grain by fine-scale etch features that greatly increase the reactive surface area of the solid. This increase in surface area is typically not accounted for in dissolution rate calculations (Stillings and Brantley, 1995). If similar channeling occurs in all olivine dissolution experiments, a significantly larger decrease in reaction rates at long reaction times is implied (see Santelli et al., 2001).

The relative reactivity of M1 and M2 sites in olivine has been considered previously. For example, Awad et al. (2000) noted that O(1) sites (Birle et al., 1968) are relatively unsaturated compared to O(2) and O(3) sites. Because M1 sites are bound to two O(1), two O(2), and two O(3) whereas M2 sites are coordinated by one O(1), one O(2), and four O(3), these authors predict preferential protonation of M1. Given the importance of protonation of metal ions in olivine in the dissolution pathway (Westrich et al., 1993), it is probable that cations will be liberated preferentially from M1 sites.

Examination of the projected olivine structure (Fig. 8) readily explains why creation of vacancies on M1 should result in planar etch pits parallel to (001). The M1 site distribution also explains the tendency to develop diamond shaped islands bounded by {110} within the (001) plane, as reported previously.

One of the most interesting observations of the prior work of Santelli et al. (2001) is the very considerable decrease in reactivity of fayalite in the presence of microorganisms (measured by accumulation of Si in solution, not by accumulation of iron, which is sequestered into secondary minerals). At pH 2, fayalite dissolution was inhibited by a factor of 5 to 50 compared to the abiotic controls. Although both the abiotic and biotic experiments were carried out in oxygenated solutions, the amount of ferric iron present in the two experiments was quite different. The inorganic rate of ferrous iron oxidation by oxygen at pH 2 is very slow, so that no significant ferric iron is present in the abiotic experiments. However, microorganisms catalyze ferrous iron oxidation. Abiotic addition of ferric iron is an excellent proxy for microbial activity, and ferric iron addition has an analogous effect on the reaction rate, even at quite low concentrations (Santelli et al., 2001). The result that olivine dissolution rates can be significantly inhibited by ferric iron may be quite important, as much natural olivine dissolution occurs under oxidizing conditions (as evidenced by the forma-

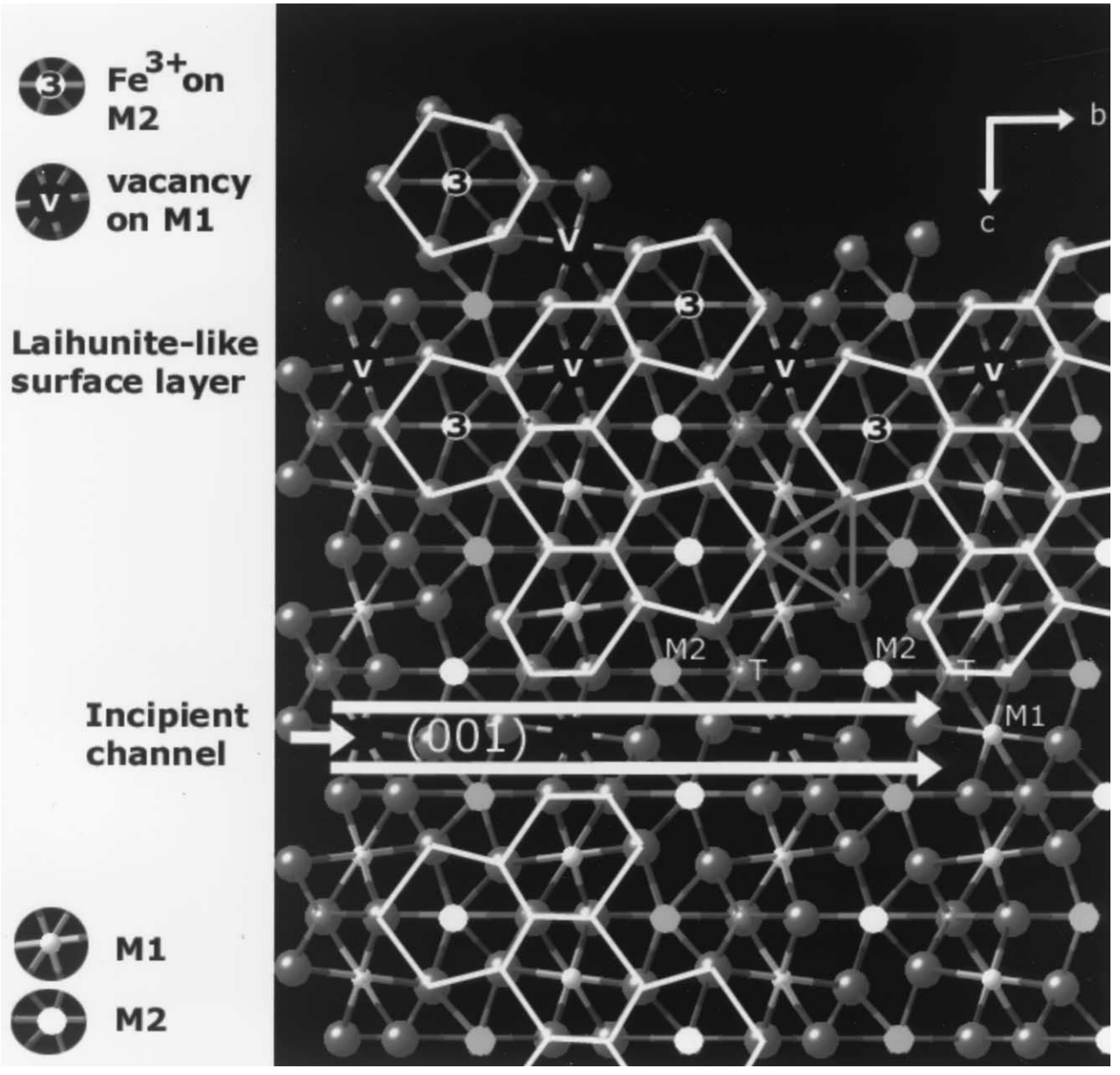

Fig. 8. Diagram showing how horizontal, (001)-bounded channels develop in fayalite (white arrows) as the result of selective removal of M1 octahedral cations. The combination of ferric iron adsorption and vacancy formation on the upper (001) surface leads to creation of laihunite-like character. White lines highlight the zig zag pattern of M2 and M1 cations characteristic of olivine.

tion of ferric iron products in direct proximity to weathered surfaces; see Smith et al., 1987).

Why does addition of relatively small quantities of ferric iron dramatically inhibit olivine dissolution? The absence of tightly adhering ferric iron oxyhydroxide coatings rules out reaction inhibition by the formation of a "diffusion inhibiting layer" (e.g., see discussion in Velbel, 1986). High-resolution TEM image details indicate olivine structure persists to within a fraction of a nanometer of (001) surfaces. This suggests that passivation of the surface is either due to specific adsorption of ferric iron to reactive surface sites or to modification of the near surface olivine structure and/or composition.

High-resolution TEM lattice fringe images of fayalite from the biologic experiments showed that the surface retains olivine-like structural characteristics, despite its greatly reduced reactivity. The only Mg-Fe olivine phase known to have greatly reduced susceptibility to dissolution is laihunite (or Mg-laihunite, Banfield et al., 1990). It has been established previously that planar defects of laihunite dramatically restrict retreat of olivine surfaces (e.g., see Figs. 17 and 19 of Banfield et al., 1990). Laihunite occurs either in zones bounded by (001) surfaces or as individual unit cells (planar defects) parallel to (001) olivine. Because laihunitized olivine presents a formidable barrier for retreat of the (001) channel surfaces, we consider

the possibility that a laihunite-like layer is forming on (001) surfaces in experiments when ferric irons are present.

Formation of a laihunite-like phase could be achieved, in part, by adsorption of ferric iron to M2 surface sites previously occupied by ferrous iron, or by oxidation of ferrous iron in M2 sites near the mineral surface. Laihunite formation also requires creation of vacancies on M1 sites. It is notable that the electronic charge distribution analysis of Awad et al. (2000) and etch formation mechanism proposed here both point to creation of surface M1 site vacancies as an inherent part of the dissolution reaction. Thus, we suggest that the combined effects of ferric iron production (or addition) and leaching of M1 octahedral cations leads to formation of an unreactive laihunite-like surface region. The "armoring" of etch surfaces as they form may explain why innumerable narrow channels rather than a few large channels appear during olivine weathering. In fact, laihunitization of the olivine surface may be an inevitable consequence of proton-promoted olivine dissolution in the presence of ferric iron.

Some support for ferric iron enrichment of olivine surfaces during dissolution is found in a brief report by Wogelius and Fraser (1996). These authors interpreted results of X-ray absorption spectroscopic experiments to suggest that olivine surfaces reacted at pH 4 were enriched in ferric iron to depths in excess of 10 nm. However, confirmation that the fayalite surface is truly laihunite-like requires detailed verification of the distribution of ferric iron and vacancy sites. This will require application of sophisticated methods sensitive to the detailed coordination environments of near-surface ions.

At initial pH 3, the measured dissolution rate in the abiotic experiments of Santelli et al. (2001) was approximately 2 orders of magnitude slower than at pH 2. This is notably different from results of prior studies, which were characterized by a much lower dependence of dissolution rate on proton activity. An important difference is that both abiotic and biologic experiments of Santelli et al. (2001) were carried out under oxidizing conditions necessary to allow for growth of *A. ferrooxidans*. At pH 3, the rate of inorganic oxidation of ferrous iron released by fayalite dissolution is considerably faster than at pH 2. Thus, we suggest that the anomalously slow pH 3 fayalite dissolution rate of Santelli et al. reflects, in large part, the inhibitory effect of ferric iron on olivine dissolution (as seen at pH 2 in biologically catalyzed, and ferric iron amended, experiments).

Formation of laihunite-like surface layers may be relevant to the question of how olivine mineral reactions contribute to support of a subsurface biosphere. In addition to the possibility that ferrous iron oxidation can be coupled to oxygen reduction in microaerophilic environments to sustain microbial growth in near neutral pH solutions (Santelli et al., 2001), Stevens and McKinley (1995) point to olivine as a source of hydrogen for microbial methanogenesis. They propose that ferrous ions in Fe-silicates reduce water to produce hydrogen. However, they do not elucidate the mineralogical details of this reaction. If laihunite-like phases can form in low-temperature aqueous environments, then laihunite may be an important byproduct of hydrogen-forming reactions. Thus, low temperature olivine surface reactions occurring during weathering may be of additional importance to understanding the workings of the deep biosphere system.

Acknowledgments—Support for this research was provided by NSF grant EAR 9317082 and DOE grant DE-FG02 to 93ER14328. Electron microscopy was carried out in the Materials Science Center, University of Wisconsin Madison. Michael Velbel and two anonymous reviewers are thanked for their constructive comments.

Associate editor: P. A. Maurice

REFERENCES

Awad A., Van Groos, F. K., and Guggenheim S. (2000) Forsteritic olivine. Effect of crystallographic direction on dissolution kinetics. *Geochim. Cosmochim. Acta.* **64,** 1765–1772.

Banfield J. F., Veblen D. R., and Jones B. F. (1990) Transmission electron microscopy of subsolidus oxidation and weathering of olivine. *Contrib Mineral. Petrol.* **106,** 110–123.

Banfield J. F., Jones B. J., and Veblen D. R. (1991) An AEM-TEM study of weathering and diagenesis, Abert Lake, Oregon. (I) Weathering reactions in the volcanics. *Geochim. Cosmochim. Acta.* **55,** 2781–2793.

Banfield J. F., Dyar M. D., and McGuire A. V. (1992) The defect microstructure of oxidized mantle olivine. *Am. Mineral.* **77,** 977–986.

Birle J. D., Gibbs G. V., Moore, P. B., and Smith, J. V. (1968) Crystal structures of natural olivines. *Am. Mineral.* **53,** 807–824.

Casey W. H., Banfield J. F., Westrich H. R., and McLaughlin L. (1993) What do dissolution experiments tell us about natural weathering? *Chem. Geol.* **105,** 1–15.

Eggleton R. A. (1984) Formation of iddingsite rims on olivine: A transmission electron microscopy study. *Clays Clay Min.* **32,** 1–11.

Fisk M. R., Giovannoni S. J., Thorseth I. H. (1998) Alteration of oceanic volcanic glass: Textural evidence of microbial activity. *Science.* **281,** 978–980.

Hoch A. R., Reddy M. M., and Drever J. I. (1996) The effect of iron content and dissolved O_2 on dissolution rates of clinopyroxene at pH 5.8 and 25°C: Preliminary results. *Chem. Geol.* **132,** 151–156.

Jakosky B. M., and Shock E. L. (1998) The Biological Potential of Mars, the Early Earth, and Europa. *J. Geophys. Res.* **103,** 19359–19364.

Janney D. E. and Banfield J. F. (1998) Cation ordering in oxidized olivine. *Am. Mineral.* **83,** 799–810.

Kondoh S., Kitamura M., and Morimoto N. (1985) Synthetic laihunite, $V_xFe^{2+}_{2-3x}Fe^{3+}_{2x}SiO_4$, an oxidation product of olivine. *Am. Mineral.* **70,** 737–746.

Liermann L. J., Kalinowski B. E., Brantley S. L., Ferry J. G. (2000). Role of bacterial siderophores in dissolution of hornblende. *Geochim. Cosmochim. Acta.* **64,** 587–602.

McCollom T. M. and Shock E. L. (1997) Geochemical constraints on chemolithoautotrophic metabolism by microorganisms in seafloor hydrothermal systems. *Geochim. Cosmochim. Acta.* **61,** 4375–4391.

Santelli C. M., Welch S. A., Westrich H. R., and Banfield J. F. (2001). Fe oxidizing bacteria and the weathering of Fe silicate minerals. *Chem. Geol.* **180,** 99–115.

Shen B., Tamada, O., Kitamura M. and Morimoto N. (1986) Superstructure of laihunite-3M. *Am. Mineral.* **71,** 1455–1460.

Siever R., and Woodford N. (1979) Dissolution kinetics and the weathering of mafic minerals. *Geochim. Cosmochim. Acta.* **43,** 717–724.

Smith K. L., Milnes A. R. and Eggleton, R. A. (1987) Weathering of basalt: formation of iddingsite. *Clays Clay Min.* **35,** 418–428.

Stevens T. O. and McKinley J. P. (1995) Lithoautotrophic microbial ecosystems in deep basalt aquifers. *Science.* **270,** 450–454.

Stillings L. L. and Brantley S. L. (1995) Feldspar dissolution at 25°C and pH 3: Reaction stoichiometry and the effect of cations. *Geochim. Cosmochim. Acta.* **59,** 1483–1496.

Thorseth I., Furnes H. and Heldal M. (1992) The importance of microbial activity in the alteration of natural basaltic glass. *Geochim. Cosmochim. Acta.* **56,** 845–850.

Thorseth I., Furnes H., and Tumyr O. (1995) Textural and chemical

effects of bacterial activity on basaltic glass: an experimental approach. *Chem. Geol.* **119,** 139–160.

Velbel M. A. (1986) Influence of surface area, surface characteristics, and solution composition on feldspar weathering rates. In *Geochemical Processes at Mineral Surfaces* (eds. J. A. Davis and K. F Hayes) vol. 323, pp. 615–634. American Chemical Society Symposium Series.

Westrich H. R., Cygan R. T., Casey W. H., Zemitis C., and Arnold G. W. (1993) The dissolution kinetics of mixed-cation orthosilcate minerals. *Am. J. Sci.* **293,** 869–893.

White A. F., and Yee A. (1985) Aqueous oxidation-reduction kinetics associated with coupled electron-cation transfer from iron containing silicates at 25°C. *Geochim. Cosmochim. Acta.* **49,** 1263–1275.

Wogelius R. A. and Fraser D. G. (1996) Surface oxidation and hydroxylation of olivine producted by reaction with aqueous solutions: an ex situ XAS (REFLEXAFS) and ERDA study. V.M. Goldschmidt Conference Journal of Conference Abstracts, Heidelberg, Germany. Cambridge Publications, p. 684.

Wogelius R. A. and Walther J. V. (1992) Olivine dissolution kinetics at near surface conditions. *Chem. Geol.* **97,** 101–112.